Temperature-dependent x-ray diffuse scattering from single crystals of $La_{2-x}Sr_xCuO_4$

W. Dmowski
Laboratory for Research on the Structure of Matter and Department of Materials Science and Engineering, University of Pennsylvania, Philadelphia, Pennsylvania 19104-6272

R. J. McQueeney
Laboratory for Research on the Structure of Matter and Department of Physics, University of Pennsylvania, Philadelphia, Pennsylvania 19104-6272

T. Egami
Laboratory for Research on the Structure of Matter and Department of Materials Science and Engineering, University of Pennsylvania, Philadelphia, Pennsylvania 19104-6272

Y. P. Feng and S. K. Sinha
Exxon Research and Engineering, Annandale, New Jersey 08801
and Advanced Photon Source, Argonne National Laboratory, Argonne, Illinois 60439

T. Hinatsu and S. Uchida
Superconductivity Course, University of Tokyo, Tokyo 103, Japan
(Received 22 August 1994; revised manuscript received 21 February 1995)

X-ray diffuse scattering from single crystals of $La_{2-x}Sr_xCuO_4$ ($x=0.10,0.15,0.20$) was studied in the vicinity of several Bragg peaks near the c^* axis as a function of temperature. While the diffuse scattering at room temperature is dominated by phonon scattering, at low temperatures residual nonphonon diffuse scattering is clearly seen. The intensity of the residual nonphonon scattering depends upon temperature and composition in a characteristic manner. It is suggested that the nonphonon scattering is due to local lattice distortions induced by charge carriers in these compounds.

I. INTRODUCTION

It has become recognized as a result of various noncrystallographic structural studies that the actual local atomic structure of high-temperature superconducting oxides is slightly deviated from the average crystallographic structure.[1] Evidence of such local deviations is provided by extended x-ray-absorption fine-structure (EXAFS) studies,[2–5] pulsed neutron atomic pair-distribution function (PDF) studies,[6–12] anomalously large x-ray and neutron thermal factors,[13] observation of IR-active modes by Raman scattering,[14] NQR measurements,[15] PAC measurement,[16] and electron diffraction.[17] The first two types of studies, as well as ion-channeling[18,19] and inelastic neutron scattering studies,[20,21] have revealed anomalous lattice behavior near the superconducting transition temperature, prompting a speculation that the lattice may be intimately involved in the superconducting phenomena. Even though some of the claims of local distortion, particularly of the split apical oxygen sites,[2,3] have been questioned,[22,23] and are still controversial, there seems to exist strong enough evidence for the presence of some significant local atomic displacements or local lattice vibrations beyond what are expected for phonon excitations.

These local atomic deviations should result in additional diffuse scattering of x rays other than thermal diffuse scattering (TDS) due to phonons. The purpose of the present study is to detect such x-ray diffuse scattering from single crystals of superconducting oxides. As will be described in this paper, our study uncovered significant nonphonon x-ray diffuse scattering intensities which depend upon composition and temperature and could be interpreted as to be originating from the charge-induced local lattice distortion. The measurements were made on $La_{2-x}Sr_xCuO_4$ ($x=0.1,0.15,0.2$) single crystals. The $La_{2-x}Sr_xCuO_4$ superconductors offer a unique opportunity to study properties as a function of doping. The system evolves from an antiferromagnetic insulator to a superconductor and then to a metal with increasing strontium content. The maximum in T_c is observed at a so-called optimum doping, at about $x=0.15$.[24] The isotope effect depends on the value of x and is minimal also at about $x=0.15$.[25] The normal-state transport properties, especially charge dynamics, are distinct from normal metals and are sensitively dependent upon composition.[26–28]

II. EXPERIMENTAL METHODS

X-ray scattering measurements were performed at the National Synchrotron Light Source (NSLS) beamline X-25. This beamline is a 27-pole wiggler line with focusing optics that produces a beam with very high flux and brilliance. The size of the x-ray beam at the sample was typically 1×1 mm^2. The scattered x rays were detected by a

Ge solid-state detector. The energy resolution of the Ge detector was 230 meV at 20 keV. Photon energy was tuned to 18 keV and pulse height analyzers were used to monitor the intensities of the scattered x rays and Sr and Cu fluorescence signals. The Sr fluorescence signal was used in order to normalize the scattering intensity, taking the Sr concentration of the sample into account. This allowed the scattering intensities from three different samples be compared directly. The measured wave-vector resolution of the system was $\sigma_x=0.0021$ Å^{-1}, $\sigma_y=0.0048$ Å^{-1}, $\sigma_z=0.0032$ Å^{-1}, where σ is a standard deviation. The incident x-ray beam was in the x-z plane and the z axis was parallel to the scattering vector $\mathbf{Q}$, $|\mathbf{Q}|=4\pi\sin\Theta/\lambda$, where Θ is the diffraction angle and λ is the wavelength of the x ray. The scattering intensity through the Bragg peak (0,0,18) in the scan $(0,0,18+\zeta)$ is shown in Fig. 1 in the logarithmic scale. The Bragg peak itself can be fitted by a Gaussian function as shown, while there is significant intensity away from the Bragg peak which is not due to the resolution effect, but represents diffuse scattering. The diffuse scattering measurements were carried out at least $6\cdot\sigma$ away from the Bragg peak in order to avoid the tail of the Bragg peak. The multiple-scattering intensities due to the combined small-angle scattering and Bragg scattering were identified and excluded from consideration. Additionally, several high-resolution measurements were performed using a Si [111] analyzer crystal to rule out possible resolution problems. In this case, the $\mathbf{Q}$ resolution was $\sigma_x=0.0010$ Å^{-1}, $\sigma_y=0.0028$ Å^{-1}, and $\sigma_z=0.0008$ Å^{-1}, respectively.

Three single crystals of $La_{2-x}Sr_xCuO_4$ ($x=0.10, 0.15, 0.20$) were grown by the floating zone method.[27] Their dimensions are $2\times2\times1$ mm^3 ($x=0.1$), $3\times4\times1$ mm^3 ($x=0.15$), and $2\times1\times1$ mm^3 ($x=0.2$) with the largest area perpendicular to the c axis, in the tetragonal notation, for $x=0.1$ and 0.2, and to the a axis for $x=0.15$. The respective superconducting temperatures are $T_c=30$ K for $x=0.10$, $T_c=35$ K for $x=0.15$, and $T_c=31$ K for $x=0.20$, as determined by the onset of the Meissner effect. The crystals were mounted in a closed-cycle displex refrigerator. Measurements were carried out from 10 K to room temperature.

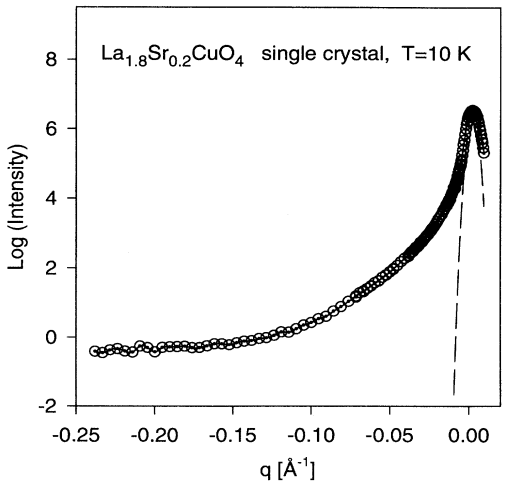

FIG. 1. X-ray scattering intensity in logarithmic scale (to base 10) in the scan along $\mathbf{Q}=(0,0,18)+\mathbf{q}$ with $\mathbf{q}\|z$ through the (0,0,18) Bragg peak. The dashed line is a Gaussian fit to the Bragg peak. Strong diffuse scattering is seen outside the Bragg peak tail.

III. RESULTS

The intensity of x-ray diffuse scattering at low temperature is weak even when the measurements are made with the wiggler beam, as shown in Fig. 1, being 7 orders of magnitude lower than the Bragg peak intensity at large q values, where $\mathbf{q}$ is the deviation of $\mathbf{Q}$ from the nearest Bragg point. Thus, it is impractical to attempt measurements over a wide range of Q space, particularly when the temperature dependence is of interest. In the present work, we focused on the diffuse scattering near the c^* axis, since the pulsed neutron PDF studies indicated significant oxygen displacements along the c axis.[1,11] Furthermore, most of the results shown here were obtained near the Bragg peaks. No extra intensities other than the background and Compton scattering intensity were detected around the forbidden diffraction peaks such as $(0,0,l=\text{odd})$. Also, negligible diffuse scattering was observed near the weak superlattice peak for the orthorhombic phase, $(0.5,0.5,l)$ in the tetragonal indices. Measurements were made around $(0,0,l)$ Bragg points with $l=6,8,10,12,14,16,18$, and $(-1,1,l)$ and $(-2,0,l)$ Bragg points with $l=14,18$ in the tetragonal indices. In this paper, we will discuss mainly the results obtained near the (0,0,18) Bragg peak. Earlier results were reported elsewhere.[29,30]

At this level of sensitivity, diffuse scattering from many crystallographic defects were observed, even though the crystal can be regarded as high quality, judging from the conventional Laue pattern or sharpness of the Bragg peaks. These scattering intensities due to defects can be easily identified since they are temperature independent and typically have a form of diffraction rods, indicating that they are due to planar defects in real space, like stacking faults. They do not form any systematic pattern near different Bragg peaks or for different crystals, except that they can be frequently found on the crystal axes.

If we denote the position of an atom in the nth unit cell $\rho_{n,\gamma}=\mathbf{R}_n+\mathbf{r}_\gamma+\mathbf{u}_{n,\gamma}$, where $\mathbf{R}_n$ is the position of the nth unit cell, $\mathbf{r}_\gamma$ is a vector pointing to the atom within the nth cell, and $\mathbf{u}_{n,\gamma}$ describes displacement field (both static and dynamic), then the diffuse x-ray scattering amplitude due to the displacement field at the momentum transfer $\mathbf{Q}$ is proportional to

$$A(\mathbf{Q})=\delta(\mathbf{Q}-\mathbf{q}-\mathbf{K})\sum_\gamma f_\gamma(Q)e^{-W_\gamma}e^{i\mathbf{K}\cdot\mathbf{r}_\gamma}\mathbf{Q}\cdot\mathbf{u}_{q,\gamma}\ , \qquad (1)$$

where $f_\gamma(Q)$ and W_γ describe the atomic scattering factor and the Debye-Waller (DW) factor, respectively, of the γth atom and $\mathbf{K}$ is the reciprocal-lattice vector.[31] $\mathbf{u}_{q,\gamma}$ is a Fourier transform of $\mathbf{u}_{n,\gamma}$:

$$\mathbf{u}_{q,\gamma}=\frac{1}{\sqrt{N}}\sum_{n}\mathbf{u}_{n,\gamma}e^{i\mathbf{q}(\mathbf{R}_n+\mathbf{r}_\gamma)} . \quad (2)$$

The diffuse scattering intensity, which is a square of the amplitude (1), is then proportional to $(\mathbf{Q}\cdot\mathbf{u})^2$. Therefore, the displacements along the c axis can be studied by observing diffuse scattering with $\mathbf{Q}$ nearly parallel to c^*.

In order to separate thermal diffuse scattering (TDS) due to phonons from the total scattering intensity, we calculated the TDS intensity [square of Eq. (1)] using the shell model. The force constants and the atomic charges in the model were chosen to reproduce the inelastic neutron-scattering data for the La_2CuO_4 single crystal by the Karlsruhe group.[32] The phonon dispersion calculated by this model is shown in Fig. 2. The calculated TDS was corrected for the DW factor[33] and the theoretical Compton scattering intensity[34] was added.

Figures 3(a) and 3(b) present intensity mapping in $(\xi,\xi,17.85)$ and $(\xi,\xi,18-\zeta)$ planes for the $x=0.15$ crystal at 10 K. In Fig. 4, the diffuse intensity for the $x=0.2$ crystal at 10 K in the $(0,\xi,18+\zeta)$ plane is shown. Similar diffuse scattering was reported recently for $La_{1.8}Sr_{0.2}NiO_4$ and $La_{1.925}Sr_{0.075}CuO_4$.[35] Figure 3(a) appears to show strong anisotropic intensity in the (1,1,0) direction just as in Ref. 35, but a closer examination indicates that the contribution from the fourfold term is not as important as it might appear, as we discuss in detail later. The calculated TDS due to phonons in $(\xi,\xi,17.85)$ and $(\xi,\xi,18-\zeta)$ planes are shown in Figs. 5 and 6. The choice of the scaling factor will be described below. At this temperature (10 K) the measured diffuse scattering intensities differ considerably from the calculated diffuse scattering intensities, and are clearly much stronger than the TDS, particularly closer to the Bragg peak.

Figures 7(a) and 7(b) present diffuse scattering intensities measured along $(0,\xi,l)$ $l=18.15,18.2,18.3,18.4$ at 300 and 10 K, respectively, for the $x=0.2$ sample. The solid lines represent the calculated TDS intensity plus the Compton scattering intensity given in the electron units per atom. Unlike at $T=10$ K, the measured and calcu-

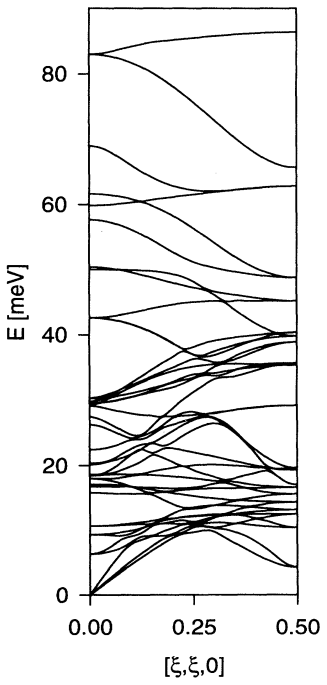

FIG. 2. Phonon dispersion calculated by the shell model for La_2CuO_4 in (100) direction (Ref. 32).

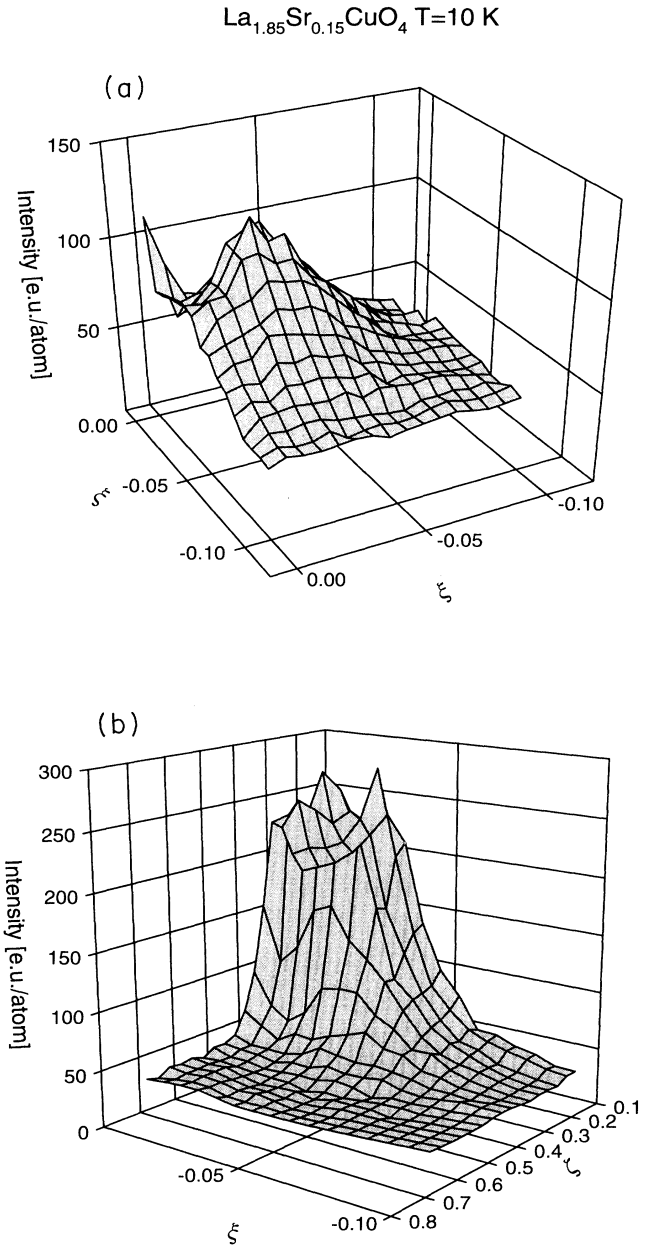

FIG. 3. Diffuse scattering for the $x=0.15$ crystal at $T=10$ K in (a) $(\xi,\xi,17.85)$ and (b) $(\xi,\xi,18-\zeta)$ planes.

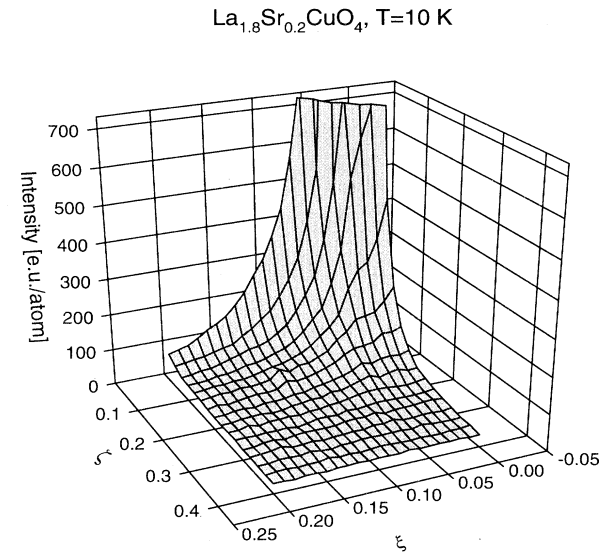

FIG. 4. Diffuse scattering in the $(0,\xi,18+\zeta)$ plane for the $x=0.2$ crystal at $T=10$ K.

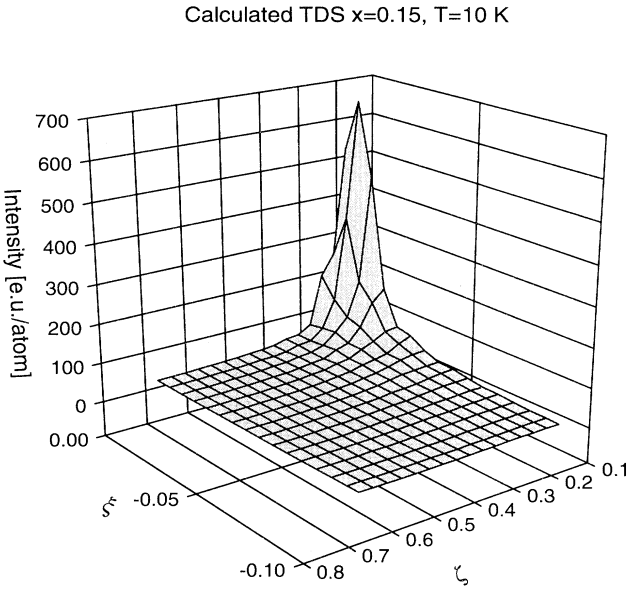

FIG. 6. Calculated TDS due to phonons in the $(\xi,\xi,18-\zeta)$ plane.

lated intensities match reasonably well at 300 K. The scaling factor for the experimental data was chosen for each crystal so that the data at 300 K match the calculated intensity at large $\mathbf{q}=\mathbf{Q}-\mathbf{K}$, where $\mathbf{K}$ is the reciprocal vector for an adjacent Bragg peak. The scattering intensity from each sample was normalized by the Sr fluorescence. By taking the Sr concentration in each sample into account, it is expected that the scaling factor be the same for all samples. This indeed is the case within 5%, confirming our interpretation that the diffuse scattering observed at room temperature is dominated by the TDS intensity. The calculated intensity agrees with the measured intensity even far away from the Bragg peak, indicating that the true instrumental background is negligibly small. As shown in Fig. 7(a), the observed diffuse scattering at room temperature is dominated by TDS. For comparison, note that in Al-doped YBCO-123 the nonphonon diffuse scattering is more intense than the TDS, even at room temperature.[36] This is not surprising, since Al was introduced to enhance vacancy ordering in that sample. The nonphonon scattering intensities discussed here are much smaller than those observed in Ref. 36.

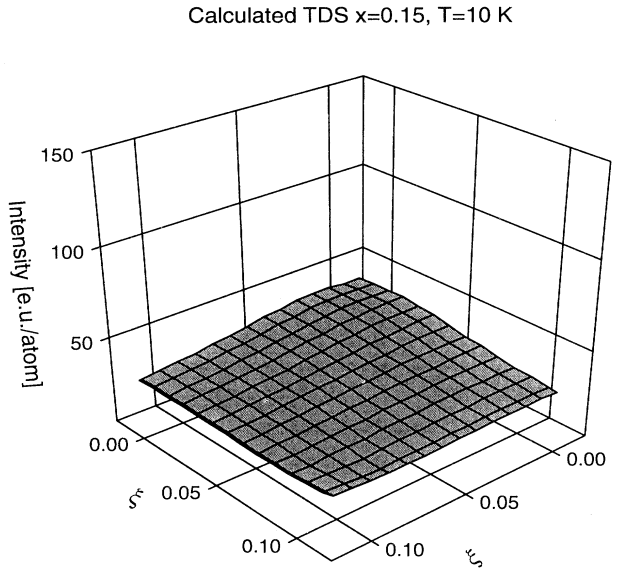

FIG. 5. Calculated TDS due to phonons in the $(\xi,\xi,17.85)$ plane.

Both the observed and calculated intensities show a characteristic dip when crossing the l axis. While the authors of Ref. 35 considered this dipping feature anomalous, this feature itself is merely a consequence of the difference between the longitudinal and transverse sound velocities. When $\mathbf{q}$ is parallel to the l axis, only the TDS due to longitudinal modes along l is observed. When $\mathbf{q}$ deviates from the l axis, we start to pick up softer transverse modes which cause an increase in the TDS intensity. Eventually, the diffuse scattering intensity diminishes at large q, since the TDS intensity is proportional to $1/q^2$ at high temperatures and $1/q$ at low temperatures. Thus, the room-temperature diffuse scattering of the $x=0.2$ sample can be almost entirely accounted for in terms of the TDS and the Compton scattering intensities, shown by a solid line in Fig. 7(a). In contrast, at 10 K, the phonon contribution accounts for only a portion of the measured intensity, and the rest, the nonphonon contribution, is actually dominant, as shown in Fig. 7(b). The same is true for other compositions, although, as will be shown later, the amount of the nonphonon intensity is composition dependent. A small sharp peak near $\xi=0$ in

Fig. 7(b) is a part of a weak rodlike diffraction feature observed nearly along the c^* axis. Its intensity and width varies with the sample, and most likely originates from stacking faults. A similar rod was sometimes observed along the a^* axis as well.

Figure 8 shows the ϕ plot, or the circular scans in the (q_x,q_y) plane with q_z being constant, with the magnitude of $\mathbf{q}$ in plane also being constant, for three compositions at 10 K (at $l=18.15$, 17.85, and 18.15). The Fourier analysis by fitting an equation,

$$I(\phi)=\sum_n A_n\cos(n\phi)\ , \tag{3}$$

shows that the $n=0$, 2, and 4 components are

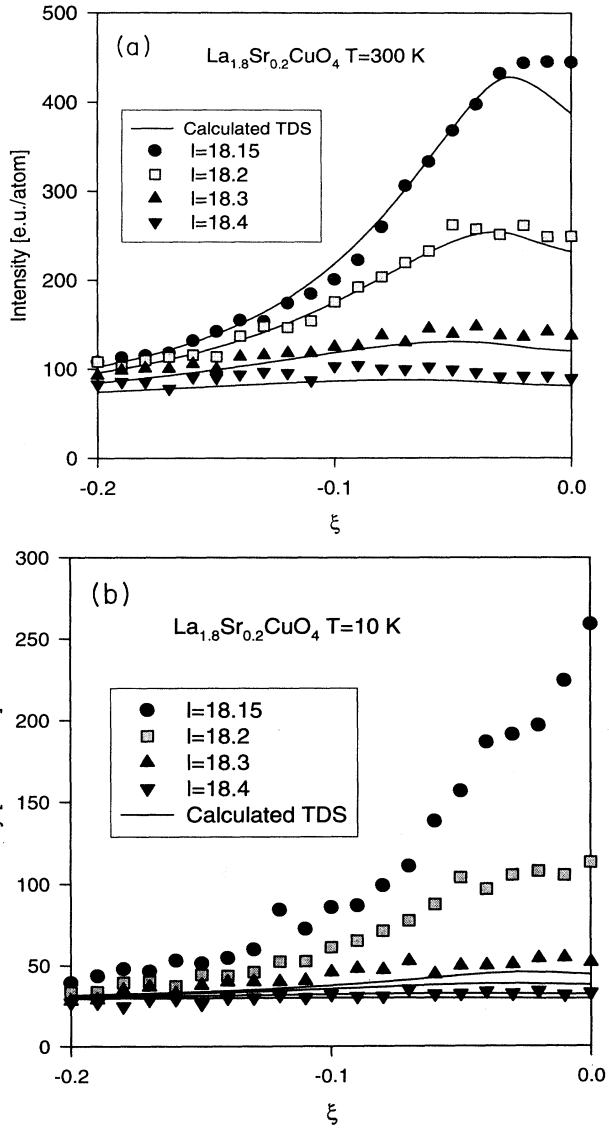

FIG. 7. Diffuse scattering intensity along (ξ,ξ,l), $l=18.15,18.2,18.3,18.4$ at (a) $T=300$ K and (b) $T=10$ K for the $x=0.2$ single crystal. Solid lines represent the calculated intensity due to phonons (TDS) plus Compton scattering. The intensity is in electron units per atom.

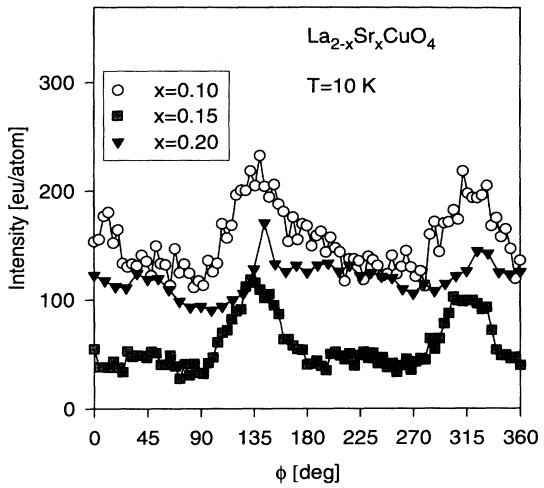

FIG. 8. Circular scans at $T=10$ K in the $l=18.15$ ($x=0.1$), $l=17.85$ ($x=0.15$), $l=18.15$ ($x=0.2$) planes with a constant magnitude of $\mathbf{q}$ (equal to 0.11 Å^{-1}). ϕ equal to zero corresponds to the $(0.05,0,l)$ point.

significantly above the noise level. The $n=0$ term is the largest and dominant at all temperatures as will be shown below. Reference 35 suggested that the $n=4$ term was dominant without quantitative analysis. Our results are not consistent with their conclusion. Also, the $n=4$ term was noted in the single-crystal neutron-scattering study of $La_2CuO_{4+\delta}$.[37] In this case, however, the $n=4$ term apparently originates from the ordering of interstitial oxygen atoms.

Figures 9 and 10 show the temperature dependence of

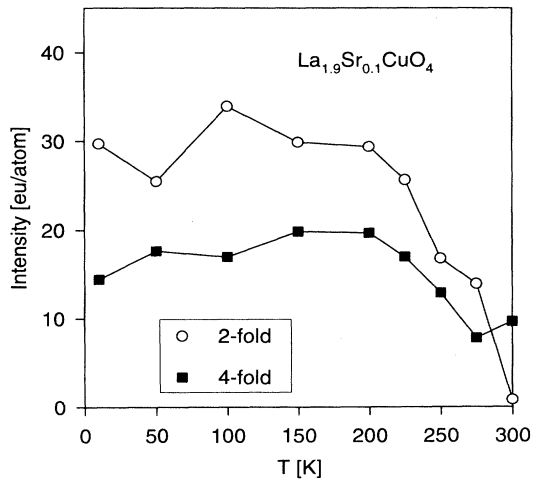

FIG. 9. The temperature dependence of the two- and four-fold terms determined from circular scans for the $x=0.1$ single crystal. The twofold component is within the margin of error from zero at 300 K, which is above the orthorhombic to tetragonal phase transition temperature.

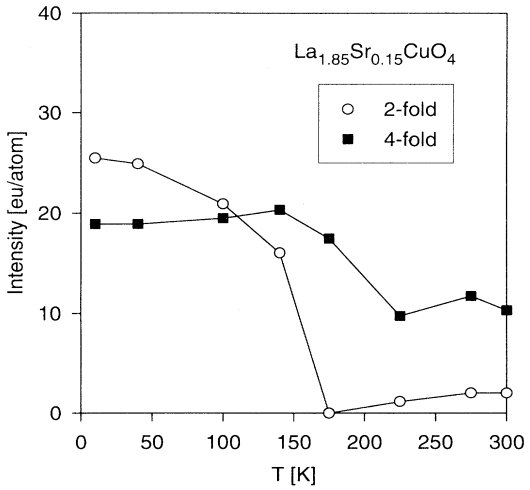

FIG. 10. The temperature dependence of the two- and fourfold terms determined from circular scans for the $x=0.15$ single crystal. The twofold component is essentially zero above 175 K, which is the orthorhombic to tetragonal phase transition temperature for this composition.

the twofold and fourfold components for the $x=0.1$ and 0.15 samples. The twofold component vanishes between 275 and 300 K or $x=0.1$, and at 175 K for $x=0.15$. For the $x=0.2$ sample, the $n=2$ component is very weak, and disappears at about 50 K. These temperatures correspond to the phase transition temperature from the tetragonal (T) phase to orthorhombic (O) phase, indicating that the $n=2$ component is a consequence of that transition, possibly due to twin boundaries. Ideally the $n=2$ term should not exist at all, even in the orthorhombic phase, because an isolated macroscopic sample should have multiple domains, or twins, with respect to the orthorhombic distortion. Upon the T/O phase transition the orthorhombic axes would be randomly chosen between the two tetragonal axes, resulting in nearly equal volume fractions for the two twins. Indeed the shape of the Bragg peaks which split upon T/O transition indicates that the two twins are nearly equally populated. It is, however, possible that the orientation of the twin boundaries are strongly anisotropic because of the sample shape or growth condition. To underscore the nonintrinsic nature of this term, the magnitude of the twofold term was observed to be slightly different each time the sample was thermally cycled through the phase transition. The twofold pattern is clearly visible also in the contour map for $La_{1.8}Sr_{0.2}NiO_4$ (Fig. 2 of Ref. 35), superimposed on the fourfold pattern.

The $n=4$ term is present above and below the T/O phase-transition temperature. However, it is possible that a part of this comes from the strain associated with the transformation. Note that the peaks at 135° and at 315° in Fig. 8 are relatively sharp with the full width at half maximum (FWHM) of about 50°. Thus they produce not only the $n=2$ but also the $n=4$ Fourier components. In addition, if there are sets of twin boundaries in orthogonal directions, each of which produces sharp peaks in the ϕ plot, it would result in a fourfold pattern. A small step in the temperature dependence of the $n=4$ term between 175 and 225 K may be an indication that a part of the $n=4$ term at low temperatures originates from the T/O phase transformation.

On the other hand, the $n=0$ component is present at all temperatures and apparently does not arise from the phase transformation. In particular, in the $x=0.2$ sample, the lattice distortion associated with the T/O phase transformation is very small, and in fact this transformation does not occur beyond $x=0.21$.[24] Therefore, it is inconceivable that the low-temperature diffuse scattering from this sample is in any way related to the T/O phase transformation. Since the diffuse intensity within the (q_x,q_y) plane can be described as a superposition of zero-, two- and fourfold terms, it is easy to separate them using scans in different directions. Scans along q_x or q_y have only the A_0 term. By summing up two diagonal scans such as along $\phi=45°$ and 135°, we can eliminate A_2 term, so that both A_0 and A_4 terms can be separately evaluated. Figure 11(a) presents scans along diagonals and q_x, while Fig. 11(b) shows the zeroth- and fourfold terms for $x=0.15$ at 10 K. It is clearly seen that the zeroth (isotropic) term is dominant in the diffuse scattering. Since the twofold term is simply a consequence of the T/O phase transformation, and is physically insignificant, we eliminated the twofold component from the data by using perpendicular scans along the two diagonal directions in the (q_x,q_y) plane. Then the calculated contribution from the TDS and Compton scattering was subtracted and the resulting *nonphonon* intensity was integrated over $\mathbf{q}$ $(\xi,\xi,18\pm0.15)$ from $\xi=0.02$ to 0.1. Figure 12 presents the temperature dependence of such an integrated intensity for three compositions. Note that the $x=0.2$ sample shows that the integrated intensity depends upon temperature particularly strongly, and is small at room temperature, as indicated by the good agreement between the measured and calculated intensities in Fig. 7(a).

IV. DISCUSSION

Various lattice defects can produce diffuse x-ray scattering. The intensity of scattering due to pointlike lattice defects such as impurities, the so-called Huang scattering,[38] is known to depend generally upon q as $1/q^2$, with weak temperature dependence that follows the Debye-Waller factor. In order to determine the power index of the q dependence, few cuts in the $(\xi,\xi,18-\xi)$ plane in the log-log scale for $x=0.15$ are plotted in Figs. 13(a) and 13(b). Theta denotes the angle that the scan makes with the c^* axis. In Fig. 13(b), the calculated phonon contribution has been subtracted. The linear fit to the data shows that the power index ν for diffuse scattering, $I\propto q^{-\nu}$, is greater than 2 for all scans even for the total intensity. Since the total intensity includes both the TDS and the nonphonon intensity, and the TDS scales as q^{-2} at high temperature and as q^{-1} at low temperatures, the power index for the nonphonon intensity has to be considerably higher than 2. Indeed after subtracting the

TDS intensity the power index is found to be much larger than 2, reaching above 4 for lower values of θ. In addition, at low values of θ, the data deviate from the linear dependence, indicating that the power index ν may be even greater along the c^* axis, although the presence of a diffraction rod probably due to stacking faults prevents us from determining the intrinsic nonphonon contribution along the c^* axis. A dependence stronger than $1/q^2$ is not expected for the diffuse scattering originating from the lattice defects. Also, as is shown in Fig. 14, the nonphonon diffuse scattering intensity is not proportional to the Sr concentration, as one would expect from the strains due to the atomic size difference between La and Sr.

The most conspicuous characteristic of the nonphonon diffuse scattering identified in this work is its temperature dependence. The temperature variation is particularly strong in the case of the $x=0.2$ sample, as shown in Fig. 12. The strong temperature dependence for the $x=0.2$ sample cannot be an artifact of the data reduction, such as the uncertainty in the scale of the TDS intensity. For instance, if we assume a temperature-independent nonphonon intensity and rescale the TDS, the overall agreement between the measured and calculated intensities is clearly far worse than the one shown in Fig. 7(a). Also, if one attempts to explain the results in terms of the temperature dependence of the phonon dispersion, not only is the observed temperature dependence[32] too small to ex-

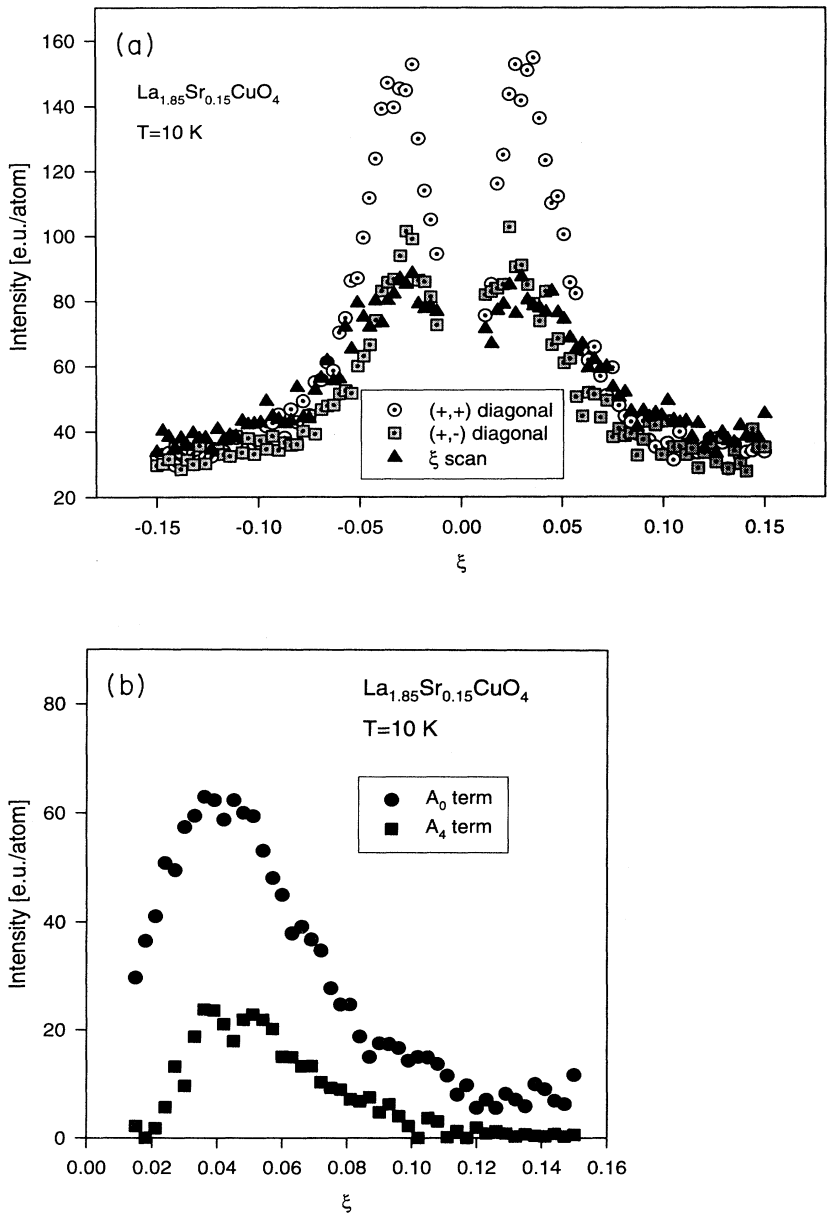

FIG. 11. (a) Diffuse intensity for scans along diagonals and ξ at 17.85 at $T=10$ K for the $x=0.15$ crystal. (b) The zero- and fourfold terms at $l=17.85$ and $T=10$ K for the $x=0.15$ single crystal.

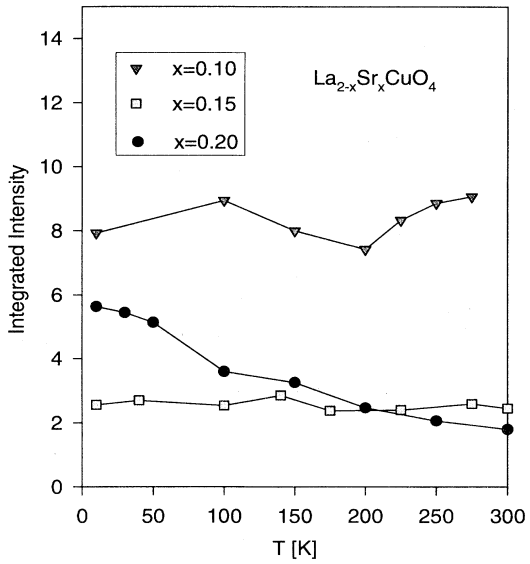

FIG. 12. The temperature dependence of the integrated intensity for three compositions. The twofold term was eliminated and the TDS and the Compton scattering intensities were subtracted. The intensity was integrated over $\mathbf{q}(\xi,\xi,18\pm0.15)$ from $\xi=0.02$ to 0.1.

plain the effect, but also one would require *softening* of the lattice at lower temperatures, which is not observed. Furthermore, according to our calculation, the TDS is nearly isotropic in the (q_x,q_y) plane. Therefore, the temperature dependence of the $n=4$ term shown in Figs. 9 and 10 cannot be due to phonons. Thus, it leaves little doubt that the residual nonphonon diffuse scattering intensity varies with temperature.

Finally, the nonphonon intensity at 10 K at the peak in Fig. 7(b) (0,0.035,18.2) is comparable in magnitude with the TDS intensity at 60 K at this q value. Therefore, the lattice distortions producing the observed diffuse scattering roughly correspond to the phonons with an amplitude of the order of 0.05 Å. If they are due to static lattice defects such as dislocations, the density of the defects necessary to explain the observed diffuse scattering intensity will be quite high, and will be inconsistent with the excellent coherence of the lattice (coherence length over 1000 Å) demonstrated by the sharpness of many of the Bragg peaks. All these considerations lead us to conclude that the origin of the nonphonon scattering cannot be extrinsic defects such as inclusions or dislocations.

It is possible that the observed strong diffuse scattering is intrinsic except for the portion related to the T/O phase transformation, and originates from the electron-lattice interaction. In nickelates, electron diffraction studies showed sharp superlattice peaks which were attributed to polaron lattice formation,[39] and the observed diffuse scattering[35] may be related to the polarons. In cuprates as well, the possibility of formation of polarons or bipolarons has been suggested.[1,3,5,11,12,40] It is therefore possible that the observed nonphonon diffuse scattering is either due directly to the mobile polarons, or more likely produced by the lattice fluctuations induced by a collective motion of polarons. Indeed, no significant elastic diffuse scattering was observed in our preliminary neutron inelastic scattering experiment, suggesting that the nonphonon diffuse scattering is probably dynamic in nature.

In this context, it is interesting to note that the temperature dependence of the nonphonon diffuse scattering is

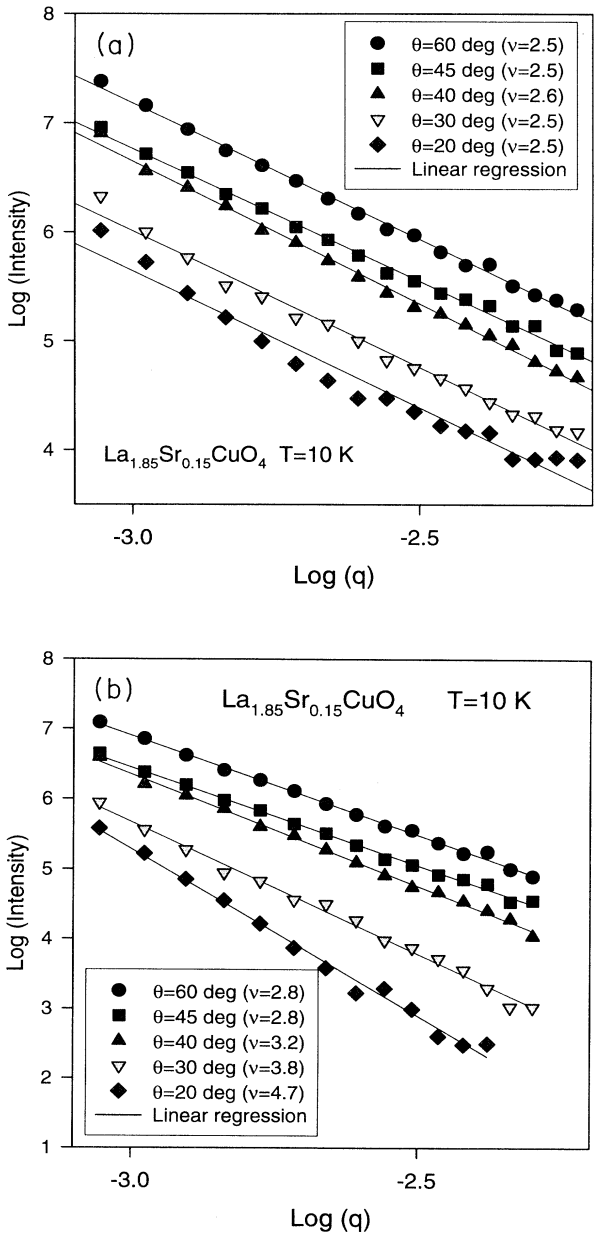

FIG. 13. Diffuse scattering for scans in the $(\xi,\xi,18-\zeta)$ plane in log-log plots (to base e) for (a) raw data, (b) after subtraction of TDS for the $x=0.15$ crystal at $T=10$ K as a function of the angle θ that $\mathbf{q}$ makes with the c^* axis. The value of ν in the inset refers to the power index, or the slope of the line.

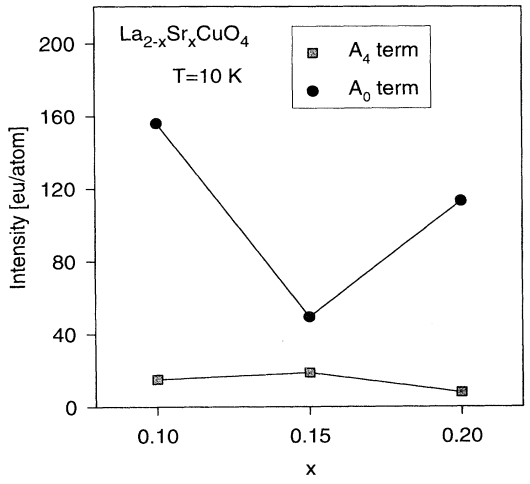

FIG. 14. The dependence on the strontium concentration of the zero- and fourfold terms, A_0 and A_4, at $T=10$ K.

qualitatively similar to that of the Hall effect.[26] The temperature dependence of the in-plane Hall coefficient, R_H, scales as $f(T/T^*)$, where T^* is a characteristic temperature below which R_H increases rapidly. The value of T^* is about 500 K for $x=0.15$ and 180 K for $x=0.2$. For $x=0.1$, T^* is estimated from the static susceptibility measurements to be about 800 K.[26,41] The strong temperature dependence of the nonphonon scattering for $x=0.2$ and the weaker dependence for $x=0.1$ and 0.15 shown in Fig. 12 are reminiscent of those of R_H. In the polaron scenario, T^* is the temperature around which the polarons are formed. Thus, the density of free carriers decreases below T^*, resulting in the increase in R_H.[42]

Another interesting point to note is the similarity in the composition dependence between the zeroth component in the diffuse scattering at 10 K shown in Fig. 14 and that of the isotope effect.[25] Both of these are minimum at $x=0.15$ where T_C is maximum. Thus they suggest that the direct electron-lattice coupling is smaller when T_C is higher. This is reasonable because self-trapped polarons with a heavy mass would be decremental to superconductivity.

This result may appear to argue against the importance of the lattice effects including polaron formation in high-temperature superconductivity. However, this can also be interpreted as an evidence that as T_C is increased, the nature of the polaron shifts from lattice polaron to electron polaron, thus reducing the polaron mass.[43,44] In purely ionic solids, a charge carrier in a polaron is screened by local ionic displacements. However, in covalent solids such as oxides the lattice deformation can cause charge transfer from one ion to another, thus leading to substantial electronic polarization which screens the charge. If this electronic component of shielding is large, proportionally less lattice deformation is required to form a polaron.

Furthermore, a recent NMR study of $La_{1.85}Sr_{0.15}CuO_4$ (Ref. 45) shows that the nuclear relaxation rate for the planar oxygen exhibits a non-Korringa behavior characteristic of the spin-gap effect. However, unlike the apical oxygen, which tracks the spin-gap-like temperature dependence of the Cu spin susceptibility detected by neutron scattering at lower temperatures, the spin-gap temperature for the planar oxygen is above 250 K. If the spin gap were to be interpreted in terms of bipolarons[42,46] the polarons must be formed above 250 K for the $x=0.15$ sample. While the present results do not allow distinction between polarons and bipolarons, they are at least compatible with this explanation.

Yet another point worth mentioning is the composition dependence of the fourfold term. As we mentioned earlier a part of this term may be related to the T/O phase transformation. Nevertheless, it is clear that the intrinsic part not related to the T/O transformation of the $n=4$ term is smaller for the $x=0.2$ sample than for others. A recent photoemission study on BISCO (Ref. 47) showed that the anisotropy of the superconducting gap in the plane has both zero- and fourfold terms. At the optimum doping the fourfold term is dominant, while in the overdoped sample the fourfold term becomes smaller and the isotropic term becomes large. If the composition dependence in BISCO could be transferred here, the composition dependencies of the A_0 and A_4 terms in Fig. 8 are qualitatively very much in parallel to those of the superconducting gap. Since the diffuse scattering reported here shows no appreciable change at T_C, it is not possible to link the symmetry of the diffuse scattering directly to the symmetry of the gap, in particular when the gap behavior in La-Sr-Cu-O is not yet known. However, it is possible that the symmetry of the preformed bipolarons is reflected in the gap symmetry.

Finally we wish to make a few comments on the fourfold pattern presented in Fig. 2 of Ref. 35. While this pattern reminds one of the intensity pattern for magnetic scattering, as the authors of Ref. 35 already have noted, they are fundamentally different. The absence of intensity near the center of this pattern is merely the consequence of the fact that the nonphonon diffuse scattering is caused almost entirely by transverse, or shear, displacements. Thus, the intensity is weak when the **Q** vector is parallel to the **q** vector, in the similar mechanism that caused a dip in the TDS intensity shown in Fig. 3. This was confirmed by studying the diffuse scattering intensity around different Bragg peaks such as $(1,1,l)$. Details of the results of such measurements will be described elsewhere.

V. CONCLUSIONS

X-ray diffuse scattering from single-crystals of $La_{2-x}Sr_xCuO_4$ ($x=0.1,0.15,0.2$) was studied as a function of temperature. The intensity of thermal diffuse scattering due to phonons was calculated by the shell model and was subtracted from the measured intensity. While the diffuse scattering at room temperature was reasonably well accounted for by TDS, at low temperatures residual nonphonon diffuse scattering was clearly seen. This result confirms that atoms are locally deviated

from the average structure in La-Sr-Cu-O beyond the level expected for lattice dynamics. The dependence of the local distortions on temperature and composition suggests that they are not due to extrinsic defects such as dislocations or substitutional defects, but are most likely induced by charge carriers as a consequence of strong electron-lattice coupling. Comparison with other properties such as Hall effect and NMR spin-lattice relaxation time leads us to speculate that the observed local lattice distortion may result from polaron formation. While this result alone does not delineate the details of the way the local electron-lattice interaction could influence high-temperature superconductivity, taken together with other evidences it points to an excellent possibility that the lattice effect plays an important role in the superconductivity of cuprates.

ACKNOWLEDGMENTS

A part of this work at the University of Pennsylvania was supported by the National Science Foundation through DMR93-00728 and DMR91-20688. The operation of the National Synchrotron Light Source is supported by the Department of Energy, Division of Materials Sciences and of Chemical Sciences. The authors are grateful to D. E. Moncton for various suggestions, in particular regarding the high-resolution scattering. They are thankful also to L. E. Berman of the NSLS beamline X-25 for his selfless assistance during the measurement. They acknowledge A. R. Bishop, E. D. Isaacs, S. Moss, M. Onellion, L. Pintschovius, W. Reichardt, G. Shirane, M. Tachiki, and K. Yamada for very useful discussions.

[1]T. Egami and S. J. L. Billinge, Prog. Mater. Sci. **38**, 359 (1994).
[2]D. Conradson and I.D. Raistrick, Science **243**, 1340 (1989).
[3]J. Mustre-de Leon, S. D. Conradson, I. Batistic, and A. R. Bishop, Phys. Rev. Lett. **65**, 1675 (1990).
[4]E. A. Stern, M. Qian, Y. Tacoby, S. M. Heald, and H. Maeda, Physica C **209**, 331 (1993).
[5]A. Bianconi, S. Della Longa, M. Missori, I. Pettiti, and M. Pompa, in *Lattice Effect in High-T_C Superconductors,* edited by Y. Bar-Yam, T. Egami, J. Mustre-de Leon, and A. R. Bishop (World Scientific, Singapore, 1992), p. 65.
[6]T. Egami, W. Dmowski, J. D. Jorgensen, D. G. Hinks, D. W. Capone, II, C. U. Segre, and K. Zhang, Rev. Solid State Sci. **1**, 101 (1987).
[7]W. Dmowski, B. H. Toby, T. Egami, M. A. Subramanian, J. Gopalakrishnan, and A. W. Sleight, Phys. Rev. Lett. **61**, 2608 (1988).
[8]B. H. Toby, T. Egami, J. D. Jorgensen, and M. A. Subramanian, Phys. Rev. Lett. **64**, 2414 (1990).
[9]S. J. L. BIllinge, T. Egami, D. R. Richards, D. G. Hinks, B. Dabrowski, J. D. Jorgensen, and K. Volin, Physica C **179**, 279 (1991).
[10]M. Arai, K. Yamada, Y. Hidaka, S. Itoh, Z. A. Bowden, A. D. Taylor, and Y. Endoh, Phys. Rev. Lett. **69**, 359 (1992).
[11]T. Egami, B. H. Toby, S. J. L. Billinge, Chr. Janot, J. D. Jorgensen, D. G. Hinks, M. A. Subramanian, M. K. Crawford, W. E. Farneth, and E. M. McCarron, in *High Temperature Superconductivity: Physical Properties, Microscopic Theory and Mechanisms,* edited by J. Ashkenazi *et al.* (Plenum, New York, 1992), p. 389.
[12]S. J. L. Billinge and T. Egami, Phys. Rev. B **47**, 14 386 (1993).
[13]K. Yvon and M. Francois, Z. Phys. B **76**, 413 (1989).
[14]S. Sugai, S. Shamoto, M. Sato, T. Ido, H. Takagi, and S. Uchida, Solid State Commun. **76**, 371 (1990).
[15]P. C. Hammel, A. P. Reyers, S.-W. Cheong, Z. Fisk, and J. E. Schirber, Phys. Rev. Lett. **71**, 440 (1993).
[16]J. Saylor and C. Hohenemser, Phys. Rev. Lett. **65**, 1824 (1990).
[17]Y. Koyama, S.-I. Nakamura, Y. Inoue, and T. Ohno, Phys. Rev. B **46**, 5757 (1992).
[18]R. P. Sharma, L. E. Rehn, P. M. Baldo, and J. Z. Liu, Phys. Rev. B **38**, 9287 (1988); Phys. Rev. Lett. **62**, 2869 (1989).
[19]T. Haga, K. Yamaya, Y. Abe, Y. Tajima, and Y. Hidaka, Phys. Rev. B **41**, 826 (1990).
[20]H. A. Mook, M. Nostoller, J. A. Harvey, N. W. Hill, B. C. Chakoumakos, and B. C. Sales, Phys. Rev. Lett. **65**, 2712 (1990).
[21]H. A. Mook, B. C. Chakoumakos, M. Nostoller, A. T. Boothroyd, and D. McK. Paul, Phys. Rev. Lett. **69**, 2272 (1992).
[22]J. D. Sullivan, P. Bordet, M. Marezio, K. Takenaka, and S. Uchida, Phys. Rev. B **48**, 10 638 (1993).
[23]J. Röhler, in *Materials and Crystallographic Aspects of HT_C-Superconductivity,* edited by E. Kaldis (Kluwar Academic, Dordrecht, 1994), p. 353.
[24]P. G. Radaelli, D. G. Hinks, A. W. Mitchell, B. A. Hunter, J. L. Wagner, B. Dabrowski, K. G. Vandervoort, H. K. Viswanathan, and J. D. Jorgensen, Phys. Rev. B **49**, 4163 (1994).
[25]M. K. Crawford, M. N. Kumchur, W. E. Farneth, E. M. McCarron, III, and S. J. Poon, Phys. Rev. B **41**, 282 (1990).
[26]H. Y. Hwang, B. Batlogg, H. Takagi, H. L. Kwo, R. J. Cava, J. K. Krajewski, and W. F. Peck, Jr., Phys. Rev. Lett. **72**, 2636 (1994).
[27]K. Tamasaku, T. Ito, H. Takagi, and S. Uchida, Phys. Rev. Lett. **72**, 3088 (1994).
[28]Y. Nakamura and S. Uchida, Phys. Rev. B **47**, 8369 (1993).
[29]W. Dmowski, T. Sendyka, T. Egami, Y.-P. Feng, S. K. Sinha, Z. Fisk, and P. C. Canfield, Bull. Am. Phys. Soc. **38**, 389 (1993).
[30]W. Dmowski, R. McQueeney, T. Egami, Y.-P. Feng, S. K. Sinha, D. E. Moncton, T. Hinatsu, and S. Uchida, Bull. Am. Phys. Soc. **39**, 185 (1994).
[31]For example, B. E. Warren, *X-Ray Diffraction* (Addison-Wesley, Reading, MA, 1969).
[32]L. Pintschovius, N. Pyka, W. Reichardt, A. Yu. Rumiantsev, N. L. Mitrofanov, A. S. Ivanov, G. Collin, and P. Bourges, Physica C **185-189**, 156 (1991).
[33]M. Braden, Ph.D. thesis, University of Köln, 1993.
[34]D. T. Cromer and J. B. Mann, J. Chem. Phys. **47**, 1892 (1967); D. T. Cromer, *ibid.* **50**, 4857 (1969).
[35]E. D. Isaacs, G. Aeppli, P. Zschack, S-W. Cheong, H. Williams, and D. J. Buttrey, Phys. Rev. Lett. **72**, 3421 (1994).
[36]X. Jiang, P. Wochner, S. C. Moss, and P. Zschack, Phys. Rev. Lett. **67**, 2167 (1991).

[37]P. G. Radaelli, J. D. Jorgensen, A. J. Schultz, B. A. Hunter, J. L. Wagner, F. C. Chou, and D. C. Johnston, Phys. Rev. B **48**, 499 (1993).
[38]K. Huang, Prog. R. Soc. **190**, 102 (1947).
[39]C. H. Chen, S.-W. Cheong, and A. S. Cooper, Phys. Rev. Lett. **71**, 2461 (1993).
[40]T. R. Sendyka, W. Dmowski, T. Egami, N. Seiji, H. Yamauchi, and S. Tanaka, Phys. Rev. B **51**, 6747 (1995).
[41]R. Yoshizaki, N. Ishikawa, H. Sawada, E. Kita, and A. Tasaki, Physica C **166**, 417 (1990).
[42]A. S. Alexandrov, Physica C **182**, 327 (1991).
[43]T. Egami, S. Ishihara, and M. Tachiki, Science **261**, 1307 (1993).
[44]T. Egami, W. Dmowski, R. J. McQueeney, T. R. Sendyka, S. Ishihara, M. Tachiki, H. Yamauchi, S. Tanaka, T. Hinatsu, and S. Uchida, Proc. SPIE, **2158**, 27 (1994).
[45]R. E. Walstedt, B. S. Shastry, and S.-W. Cheong, Phys. Rev. Lett. **72**, 3610 (1994).
[46]A. S. Alexandrov, A. M. Bratkovsky, and N. F. Mott, Phys. Rev. Lett. **72**, 1734 (1994).
[47]J. Ma, C. Quitmann, R. J. Kelly, H. Berger, G. Margaritondo, and M. Onellion, Science **267**, 862 (1995).

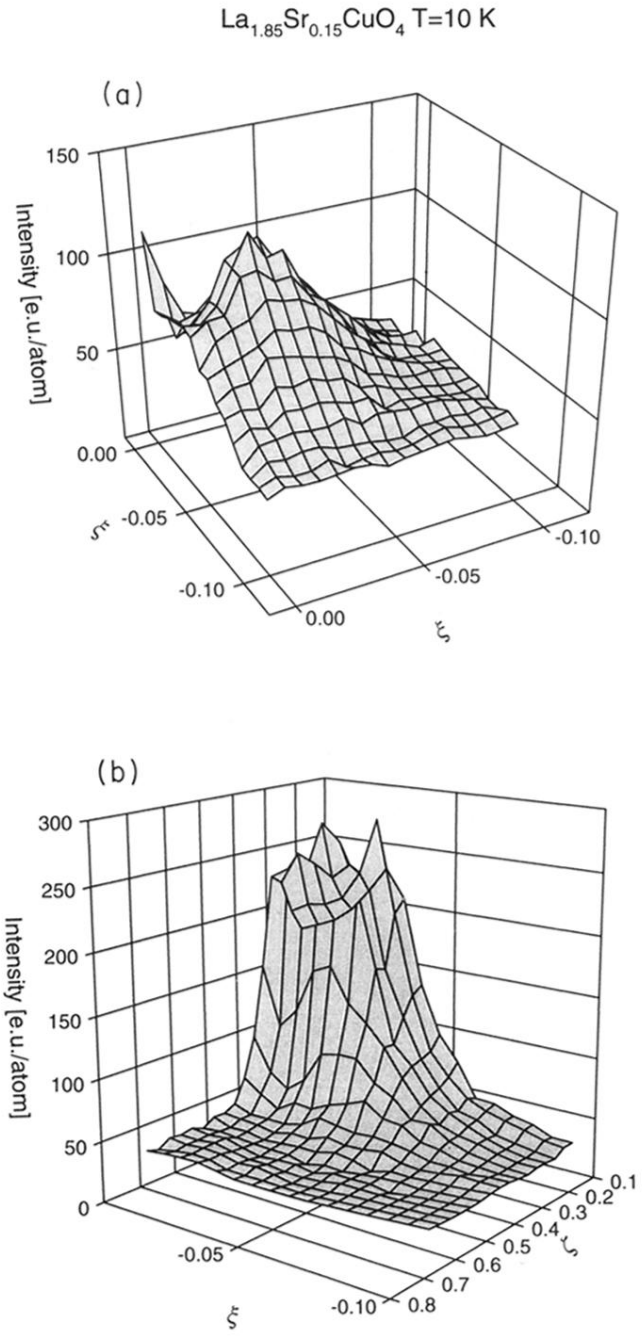

FIG. 3. Diffuse scattering for the $x = 0.15$ crystal at $T = 10$ K in (a) $(\xi, \xi, 17.85)$ and (b) $(\xi, \xi, 18 - \zeta)$ planes.

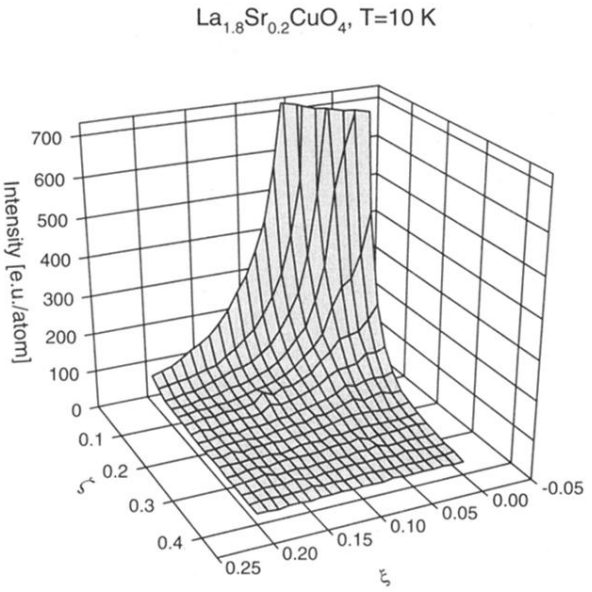

FIG. 4. Diffuse scattering in the $(0,\xi,18+\zeta)$ plane for the $x=0.2$ crystal at $T=10$ K.

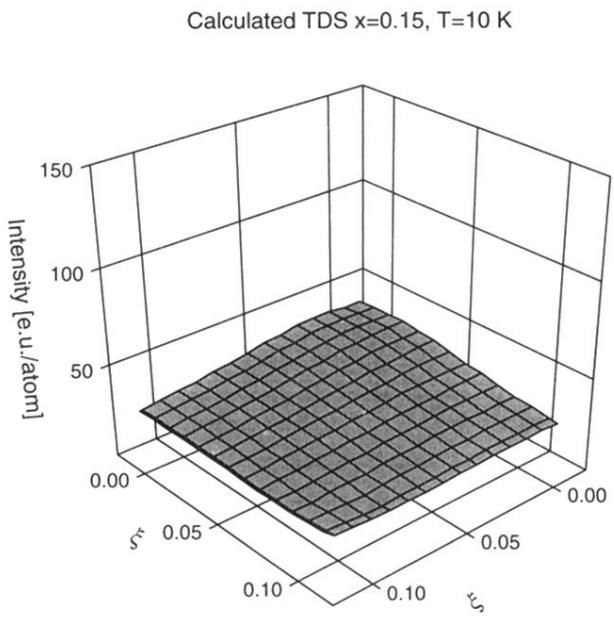

FIG. 5. Calculated TDS due to phonons in the $(\xi,\xi,17.85)$ plane.

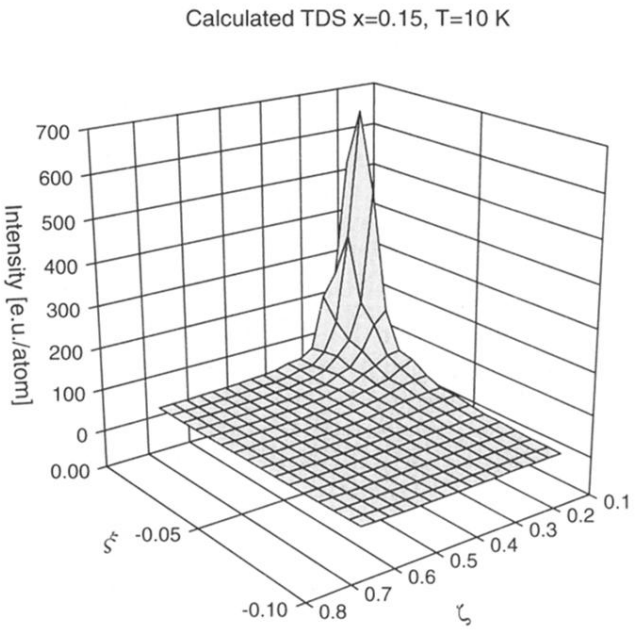

FIG. 6. Calculated TDS due to phonons in the $(\xi,\xi,18-\zeta)$ plane.